Available online at www.sciencedirect.com
SCIENCE DIRECT®
Journal of Computational Physics 191 (2003) 328–339
JOURNAL OF COMPUTATIONAL PHYSICS
www.elsevier.com/locate/jcp

Short Note

A new modification of the immersed boundaries method for fluid–solid flows: moderate Reynolds numbers

A. Vikhansky *

Department of Chemical Engineering, University of Cambridge, Pembroke Street, Cambridge CB2 3RA, UK

Received 22 October 2002; received in revised form 4 June 2003; accepted 11 June 2003

Abstract

In this study we consider a combination of an interpolation technique with the D'Alambert principle that allows the direct numerical simulation of fluid-solid flows on a regular rectangular grid. The method models a no-slip boundary with the second-order accuracy interpolation scheme without explicit calculation of the forces that the particles exert at the fluid. The method is applicable for a wide range of Reynolds numbers from creeping flows up to $Re \approx 100$.

1. Introduction

In this study we consider a method that allows the direct numerical simulation of fluid–solid flows on a regular rectangular grid without explicit calculation of the forces that the particles exert at the fluid. The no-slip boundary conditions at the solid–fluid interface are satisfied automatically. The combination of an interpolation technique with the D'Alambert principle allows an efficient numerical realization of the suggested numerical method.

Direct numerical simulation of solid–liquid flow is a difficult task since the domain occupied by the fluid is irregular and changes with motion of the particles. Also, the particles are advected by the fluid and exert forces at the fluid, so the body–liquid interaction requires calculation of the fluid stress (i.e., derivatives of the flowfield) at the fluid–solid interface. Such an approach was realized in the arbitrary Lagrangian–Eulerian (ALE) technique (see e.g. [1] and references therein), which is based on automatic generation of an unstructured finite element body-fitted mesh at each time step of the numerical algorithm. Since flow simulations on an unstructured mesh are still a challenging problem for today's computers, methods that avoid generation of a body-fitted mesh and do not require explicit calculation of a stress tensor are preferred.

During the last decade the lattice Boltzmann method has become a useful tool for studying dynamics of suspensions at low and moderate Reynolds numbers (a comprehensive review is in [2]). Another numerical technique that allows simulation of arbitrary Reynolds number flows in complex geometries on

* Tel.: +44-1223-334786.
E-mail address: av277@cam.ac.uk (A. Vikhansky).

0021-9991/$ - see front matter
doi:10.1016/S0021-9991(03)00313-9

non-body-fitted grids is the immersed boundaries method. It was demonstrated recently that this method has lower RAM and CPU-time requirements than more complicated boundary-fitted solvers [3].

The general idea of the immersed boundaries method [4] is to solve the equations for liquid velocity both inside and outside the moving boundaries, while the fluid and particle velocities are matched by forces distributed along the boundary (in the most recent variants of this method the forces are distributed over the entire region occupied by the particle). In the original paper by Peskin [4] (see also [5]) the interaction between a fluid and immersed solids is accounted for by a penalty term that makes the equations stiff and imposes restrictions on the time step. Recently, similar forcing was performed using a duality method. Distributed-Lagrange-multiplier (DLM) method [6,7] was developed and extensively applied to different particulate flows. In this method the variational equations for a fluid flow are solved on a regular grid, and the constraints of rigid-body motion of a fluid inside the particles are enforced by distributed Lagrange multipliers.

The similarity between the above two methods is due to the similarity between penalty and duality methods. One can minimize a function $f(\vec{x})$ under a constraint $g(\vec{x}) = 0$ either by penalty or duality methods. Penalty method yields the following minimization problem: $f(\vec{x}) + r(g(\vec{x}))^2 \to \min$ and $\nabla f(\vec{x}) + 2rg(\vec{x})\nabla g(\vec{x}) = 0$ in the location of the minimum, while the duality technique leads to a modified minimization problem $f(\vec{x}) + \lambda g(\vec{x}) \to \min$ and $\nabla f(\vec{x}) + \lambda \nabla g(\vec{x}) = 0$. Comparison of the above formulas shows that $2rg(\vec{x}) \to \lambda$ as penalty parameter r goes to infinity, i.e., the penalty method and the method of Lagrange multipliers are different realization of the same forcing scheme.

In the present study we suggest a variant of the immersed boundary method that does not require any explicit forcing either by the penalty method or by calculation of Lagrange multipliers. The key idea of the proposed method is a combination of the interpolation technique considered in [3,8] with a variational principle. Owing to the special treatment of near-boundary points, the constraints of rigid-body motion of fluid inside the region occupied by the particles are satisfied automatically, while the force interaction between the fluid and the immersed particles is captured implicitly by the principle of virtual work. Therefore, the problem is reduced to a sequence of unconstrained minimization problems, while the DLM method treats particle–fluid interaction via more computationally expensive constrained variational equations.

2. Variational formulation of the problem and interpolation scheme

Consider for simplicity a single disc Γ with radius R immersed into a space domain Ω filled with an incompressible viscous fluid with density ρ_f and viscosity μ (Fig. 1). The disc is made of homogeneous material with density ρ_s, the mass of the disc is $M = \rho_s \pi R^2$, and its moment of inertia $I = 1/2\rho_s \pi R^4$. The

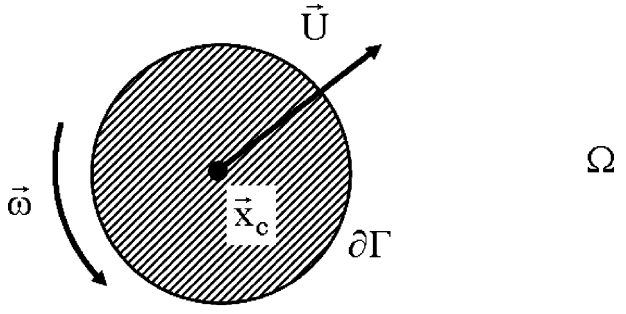

Fig. 1. Schematic view of a two-dimensional cavity with one rigid disc.

center of the disc, its axial and angular velocities are $\vec{x}_c(t)$, $\vec{U}$, and $\vec{\omega}$, respectively (angular velocity is orthogonal to the flow). The boundary of the disc is $\partial\Gamma(t)$. The acceleration of the external body force acting at the system is $\vec{g}$. The starting point of our numerical method is the virtual power principle [6]:

$$\int_{\Omega\setminus\Gamma}\left[\rho_f\left(\frac{\partial\vec{u}}{\partial t}+\left(\vec{u}\cdot\nabla\right)\vec{u}-\vec{g}\right)\cdot\delta\vec{u}+\mu\left(\nabla\vec{u}:\nabla\delta\vec{u}\right)-p\nabla\cdot\delta\vec{u}\right]\mathrm{d}\Omega + M\left(\frac{\mathrm{d}\vec{U}}{\mathrm{d}t}-\vec{g}\right)\cdot\delta\vec{U}+I\frac{\mathrm{d}\vec{\omega}}{\mathrm{d}t}\cdot\delta\vec{\omega}=0. \tag{1}$$

$$\begin{aligned}&\nabla\cdot\vec{u}=0,\quad \nabla\cdot\delta\vec{u}=0,\\ &\vec{u}|_\Gamma=\vec{U}+\vec{\omega}\times(\vec{x}-\vec{x}_c),\quad \delta\vec{u}|_\Gamma=\delta\vec{U}+\delta\vec{\omega}\times(\vec{x}-\vec{x}_c),\end{aligned} \tag{2}$$

where δ denotes variation of the corresponding variable and $\vec{u}(t,\vec{x})$ and $p(t,\vec{x})$ are the velocity and pressure of the fluid, respectively. The first term in Eq. (1) describes inertia of the fluid, the second term accounts for viscous dissipation, and the third is virtual work due to compression/expansion of the fluid. The last two terms describe linear and angular inertia of the disc.

The velocity field inside the disc is $\vec{u}=\vec{U}+\vec{\omega}\times(\vec{x}-\vec{x}_c)$, thus, the disc–inertia term in Eq. (1) can be split as

$$M\left(\frac{\mathrm{d}\vec{U}}{\mathrm{d}t}-\vec{g}\right)\cdot\delta\vec{U}+I\frac{\mathrm{d}\vec{\omega}}{\mathrm{d}t}\cdot\delta\vec{\omega}=\left(1-\frac{\rho_f}{\rho_s}\right)\left[M\left(\frac{\mathrm{d}\vec{U}}{\mathrm{d}t}-\vec{g}\right)\cdot\delta\vec{U}+I\frac{\mathrm{d}\vec{\omega}}{\mathrm{d}t}\cdot\delta\vec{\omega}\right] +\frac{\rho_f}{\rho_s}\int_\Omega\rho_s\left(\frac{\partial\vec{u}}{\partial t}+\left(\vec{u}\cdot\nabla\right)\vec{u}-\vec{g}\right)\cdot\delta\vec{u}\,\mathrm{d}\Omega.$$

Since the flow inside the disc is incompressible and does not dissipate energy, insertion of the above formula into Eq. (1) yields:

$$\int_\Omega\left[\rho_f\left(\frac{\partial\vec{u}}{\partial t}+\left(\vec{u}\cdot\nabla\right)\vec{u}-\vec{g}\right)\cdot\delta\vec{u}+\mu\left(\nabla\vec{u}:\nabla\delta\vec{u}\right)-p\nabla\cdot\delta\vec{u}\right]\mathrm{d}\Omega + \left(1-\frac{\rho_f}{\rho_s}\right)\left[M\left(\frac{\mathrm{d}\vec{U}}{\mathrm{d}t}-\vec{g}\right)\cdot\delta\vec{U}+I\frac{\mathrm{d}\vec{\omega}}{\mathrm{d}t}\cdot\delta\vec{\omega}\right]=0. \tag{1'}$$

Eq. (1′) after applying Gauss theorem implies Navier–Stokes equations

$$\left\{\rho_f\left(\frac{\partial\vec{u}}{\partial t}+\left(\vec{u}\cdot\nabla\right)\vec{u}-\vec{g}\right)+\nabla p-\mu\Delta\vec{u}\right\}\cdot\delta\vec{u}=0,\quad \text{for } \vec{x}\in\Omega\setminus\Gamma,$$

force balance over the disc

$$\int_\Gamma\left[\rho_f\left(\frac{\partial\vec{u}}{\partial t}+\left(\vec{u}\cdot\nabla\right)\vec{u}-\vec{g}\right)\cdot\delta\vec{U}\right]\mathrm{d}\Gamma+\left(1-\frac{\rho_f}{\rho_s}\right)\left[M\left(\frac{\mathrm{d}\vec{U}}{\mathrm{d}t}-\vec{g}\right)\cdot\delta\vec{U}\right] +\int_{\partial\Gamma}\left(\mu\frac{\partial\vec{u}}{\partial n}-p\vec{n}\right)\cdot\delta\vec{U}\,\mathrm{d}(\partial\Gamma)=M\left(\frac{\mathrm{d}\vec{U}}{\mathrm{d}t}-\vec{g}\right)\cdot\delta\vec{U}+\int_{\partial\Gamma}\left(\mu\frac{\partial\vec{u}}{\partial n}-p\vec{n}\right)\cdot\delta\vec{U}\,\mathrm{d}(\partial\Gamma)=0,$$

and moment balance over the disc

$$\int_\Gamma \left[\rho_f\left(\frac{\partial\vec{u}}{\partial t}+\left(\vec{u}\cdot\nabla\right)\vec{u}\right)\cdot\delta\vec{\omega}\times\left(\vec{x}-\vec{x}_c\right)\right]\mathrm{d}\Gamma+\left(1-\frac{\rho_f}{\rho_s}\right)\left[I\frac{\mathrm{d}\vec{\omega}}{\mathrm{d}t}\cdot\delta\vec{\omega}\times\left(\vec{x}-\vec{x}_c\right)\right]$$
$$+\int_{\partial\Gamma}\mu\frac{\partial\vec{u}}{\partial n}\cdot\delta\vec{\omega}\times\left(\vec{x}-\vec{x}_c\right)\mathrm{d}(\partial\Gamma)=I\frac{\mathrm{d}\vec{\omega}}{\mathrm{d}t}\cdot\delta\vec{\omega}\times\left(\vec{x}-\vec{x}_c\right)+\int_{\partial\Gamma}\mu\frac{\partial\vec{u}}{\partial n}\cdot\delta\vec{\omega}\times\left(\vec{x}-\vec{x}_c\right)\mathrm{d}(\partial\Gamma)=0.$$

In the above formulas we have used the relation that is valid inside the disc $\partial\vec{u}/\partial t+(\vec{u}\cdot\nabla)\vec{u}=\vec{U}+\dot{\vec{\omega}}\times(\vec{x}-\vec{x}_c)$. Thus, the above variational principle can be applied to simulation of particle flow interaction.

The suggested numerical procedure is as follows. We calculate the positions of the disc $\vec{x}_c$ at times $t_n=n\Delta t$, while the velocities are calculated at semi-integer moments $t_n=(n+1/2)\Delta t$. Note that the proposed procedure can be easily implemented with the variable time step. First, an intermediate position is calculated as

$$\tilde{x}(t+\Delta t/2)=\vec{x}(t)+\Delta t/8\left[7\vec{U}(t-\Delta t/2)-3\vec{U}(t-3\Delta t/2)\right].$$

Then, for the determined particle positions, Eqs. (1′) and (2) for pressure p and velocities $\vec{u},\vec{U},\vec{\omega}$ are solved by operator-splitting method [6]. We used finite-difference method on a staggered five-point stencil as follows. Variational problem (1′) and (2) is split into the following three steps:

(1) The continuity condition is enforced at the pressure-correction step

$$\vec{u}^*=\vec{u}^n-(\Delta t)\left(\nabla p^{n+1}\right).$$

Substituting the latter equation in the first of Eq. (2) yields the Poisson equation for p^{n+1}:

$$\nabla\cdot\vec{u}^*=0=\nabla\cdot\vec{u}^n-(\Delta t)\left(\Delta p^{n+1}\right). \tag{3}$$

(2) The advection step:

$$\frac{\vec{u}^{**}-\vec{u}^*}{\Delta t}=-\left(\vec{u}^*\cdot\nabla\right)\vec{u}^*. \tag{4}$$

(3) The pseudo-Stokes step that is a solution of a following quadratic minimization problem:

$$\Phi(\vec{u}^{n+1},\vec{U}^{n+1},\vec{\omega}^{n+1})=\int_\Omega\left\{\frac{\rho_f}{2\Delta t}(\vec{u}^{n+1}-\vec{u}^{**}-\Delta t\vec{g})^2+\frac{\mu}{2}\left|\nabla\vec{u}^{n+1}\right|^2\right\}\mathrm{d}\Omega$$
$$+\left(1-\frac{\rho_f}{\rho_s}\right)\left[\frac{M}{2\Delta t}(\vec{U}^{n+1}-\vec{U}^n-\Delta t\vec{g})^2+\frac{I}{2\Delta t}(\vec{\omega}^{n+1}-\vec{\omega}^n)^2\right]\to\min. \tag{5}$$

While in the case $\rho_s<\rho_f$ the coefficient near $\vec{U}$ and $\vec{\omega}$ in Eq. (5) becomes negative, the functional (5) remains positively defined with respect to these variables. Note that the terms that account for the inertia of the particle read:

$$\int_\Gamma\frac{\rho_f}{2\Delta t}(\vec{u}^{n+1}-\vec{u}^{**})^2\mathrm{d}\Gamma+\left(1-\frac{\rho_f}{\rho_s}\right)\left[\frac{M}{2\Delta t}(\vec{U}^{n+1}-\vec{U}^n)^2+\frac{I}{2\Delta t}(\vec{\omega}^{n+1}-\vec{\omega}^n)^2\right],$$

where the integration is performed over the region occupied by the particle, and $\vec{u}^{n+1} = \vec{U}^{n+1} + \vec{\omega}^{n+1} \times (\vec{x} - \vec{x}_c)$ for $\vec{x} \in \Gamma$.

The main idea of the suggested variant of the immersed boundary method that is proposed in this study is illustrated in Fig. 2. At the grid points that are far from the body the central difference approximation of dissipation term in Eq. (5) reads:

$$|\nabla u|^2 \,\mathrm{d}x\,\mathrm{d}y \approx \frac{h^2}{2}\left(\frac{(u_{ij}-u_{i-1j})^2}{h^2}+\frac{(u_{ij}-u_{i+1j})^2}{h^2}+\frac{(u_{ij}-u_{ij-1})^2}{h^2}+\frac{(u_{ij}-u_{ij+1})^2}{h^2}\right)$$
$$=\frac{1}{2}\Big((u_{ij}-u_{i-1j})^2+(u_{ij}-u_{i+1j})^2+(u_{ij}-u_{ij-1})^2+(u_{ij}-u_{ij+1})^2\Big).$$

Thus, at the points the closest to the boundary, the first term in the above expression is replaced by

$$h^2\eta\frac{\big(u_{ij}-(U-\omega(x-x_c))\big)^2}{(\eta h)^2}=\frac{\big(u_{ij}-(U-\omega(x-x_c))\big)^2}{\eta}. \tag{6}$$

Here h is the step of the grid and η is the dimensionless distance from the ith node to the surface of the disc. Since Eq. (6) is based on linear interpolation of flow field, it requires the mesh to be fine so that the linearized velocity is accurate [3]. Thus, the applicability of this method to direct simulation of two phase turbulent flows should be subject of additional investigations.

When $\eta = 1$, i.e., the distance from the ith node to the surface is equal to the step of the grid, the dissipation rate given by Eq. (6) is identical to that obtained by central difference stencil. The velocities in the nodes that are inside the disc are set equal to the velocity of the body in these points. As one can see, the

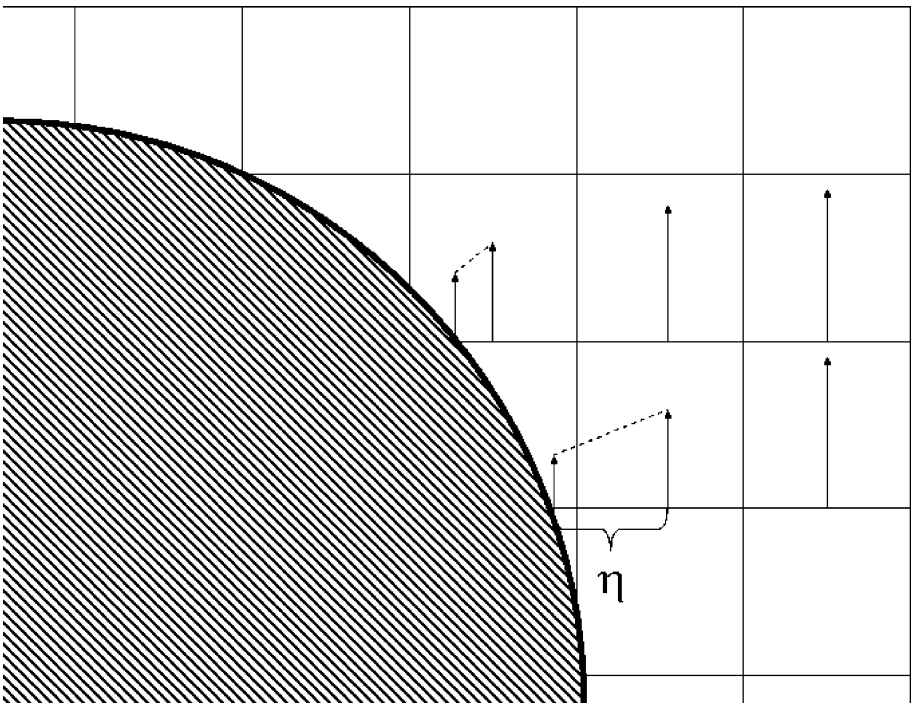

Fig. 2. Scheme of the immersed boundary method.

interpolation procedure does not explicitly use the circular shape of the disc, thus, it can be easily extended to bodies of arbitrary configuration as well as to a three-dimensional geometry.

In liquid–solid systems lubrication forces prevent the particles from colliding. Since immersed boundary method cannot properly resolve the flowfield between two near-touching particles, an artificial repelling force that accounts for the lubrication effects must be activated at close range. The collision strategy commonly used by many authors is to introduce a short-range repulsive potential that prevents particle–particle or particle–wall interpenetration [6]. If the distance between two particles is less than some small value $r' \approx 1.5h$, we penalized (4) by

$$F\left(\vec{U}_i, \vec{U}_j\right) = \frac{M_i M_j}{\varepsilon}\left(\left|\vec{x}_i + \Delta t\vec{U}_i - \vec{x}_j - \Delta t\vec{U}_j\right| - R_i - R_j - r'\right)^2,$$

where ε is a small penalty parameter. If the particle approaches a wall, a fictitious particle of the same mass and diameter that locates symmetrically with respect to the wall is introduced in order to prevent the particle–wall collision. Note, that extension of the above described collision strategy for arbitrary-shaped particles is a rather complex task since it requires evaluation of particle–particle distance.

Once the velocities are calculated we move the particles accordingly to

$$\vec{x}(t + \Delta t) = \vec{x}(t) + \Delta t\vec{U}(t + \Delta t/2).$$

3. Results and discussion

In the first test case we considered the motion of a line of neutrally buoyant particles in pressure-driven Poiseuille flow (Fig. 3). Previously, this case was simulated by two different methods, namely, lattice Boltzmann method [9] and DLM method [7]. The parameters computed in these works almost coincide and we can regard these results as "exact." The computational domain is a 1×1 square, the diameter of the disc is 0.25. The flow is periodic in the horizontal direction. Initially, the particle is at rest and the initial vertical

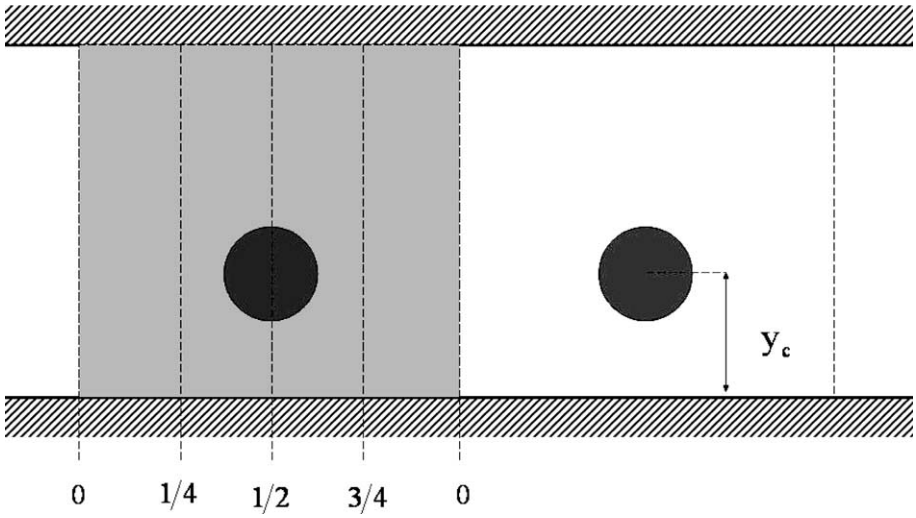

Fig. 3. Domain of computation for a line of cylinders. The periodic boundary conditions with a constant pressure drop are imposed at the lateral boundaries of the 1×1 cell.

coordinate of the center of the disc is $y_c = 0.4$. We have used a coarse 40×40 staggered mesh, thus the diameter of the disc is equal to 10 increments of the grid. The time step is $\Delta t = 0.5h/u_{max}$, where u_{max} is the maximum velocity in the computational domain. We used a central difference scheme for the convective term in Eq. (4). The minimization problem (5) was solved by a block over-relaxation method as follows. For a frozen $\vec{u}$ the functional Φ was minimized with respect to $\vec{U}$ and $\vec{\omega}$ and then a new value of $\vec{u}$ was calculated by one line-relaxation iteration and so on until convergence. This minimization procedure, performs well for coarse meshes (about 40×40) but becomes increasingly slow as the mesh size decreases. Since the functional Φ is quadratic, the calculation time can be significantly reduced by application of much more effective conjugated gradient methods.

As the flow proceeds further the particle migrates laterally and reaches a stable position (Segré–Silberberg effect). Fig. 4 shows the profiles of the fluid velocity in the horizontal direction at different relative positions. At $x = 0$ the profile is almost parabolic, at $x = 1/4$ and $x = 3/4$ the profile is distorted due to presence of the disc. At $x = 1/2$ velocity is maximum at the centerline of the channel and the linear segment belongs to the part of the flow that is occupied by the disc. Pressure around the disc contour is presented in Fig. 5. Since solid-body motion satisfies the continuity conditions, the source term in Poisson Eq. (3) is zero inside the cylinder. Thus both maxima and minima of the pressure are at the boundary of the disc. The comparison between the computed parameters and those from [7,9] is presented in Fig. 6. As one can see, the dimensionless pressure drop, equilibrium lateral position, and disc velocity to mean velocity ratio deviate from the values in [7,9] at most by 5%. The calculated angular velocity is overestimated by about 37%. We believe it is possibly due to the coarse mesh used in these computations. The results obtained on 60×60 mesh for $Re \approx 15$ are in better agreement with [7,9].

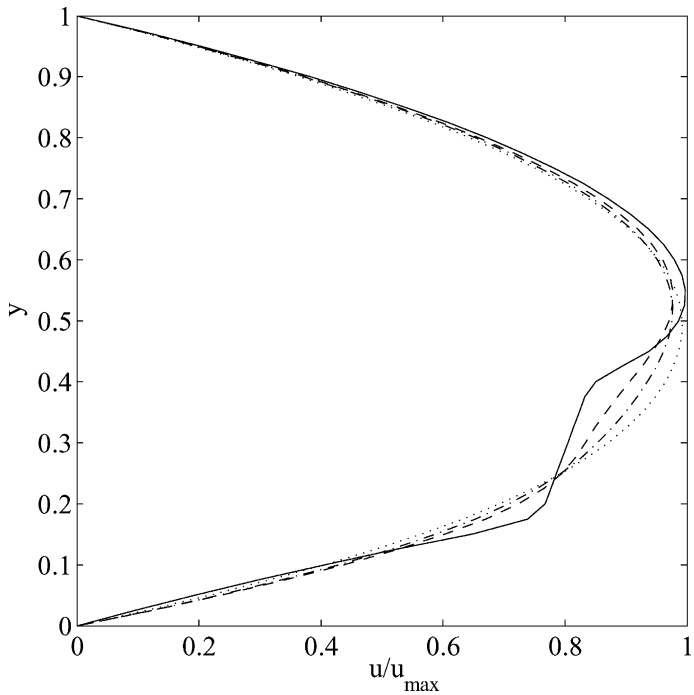

Fig. 4. Velocity profiles at $Re = 14.69$ for different sections of the channel: 0, dotted line; 1/4, dash-dotted line; 1/2, solid line; 3/4, dashed line.

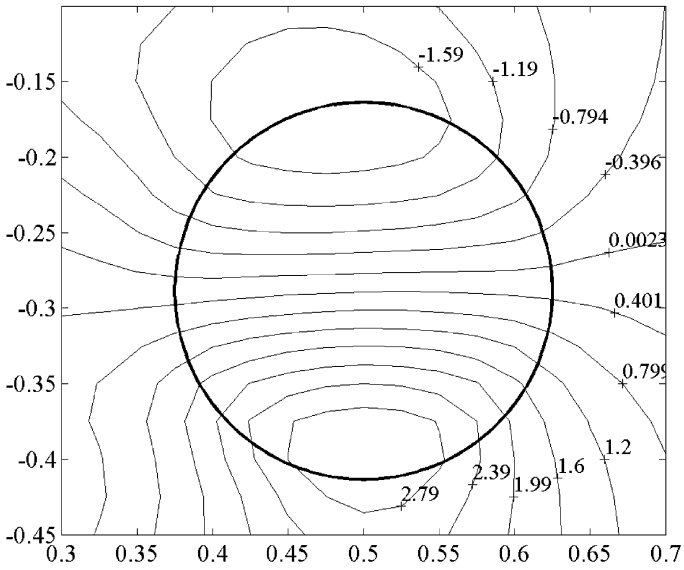

Fig. 5. Distribution of dimensionless pressure $P/\rho\langle u\rangle^2$ at $Re = 14.69$.

Another example that demonstrates the performance of the method is presented in Fig. 7. Two light discs ($\rho_s/\rho_f = 0.5$, $R = 0.2$) are trapped by the two symmetrical vortices in a lid-driven cavity. Due to the reduced density the discs are in equilibrium at the centers of the vortices even under the action of gravity, which destroys the symmetry of the flow. Due to the motion of the walls the pressure is higher near the right corners of the cavity and smaller near the left corners. Thus, in order to compensate for the buoyancy force,

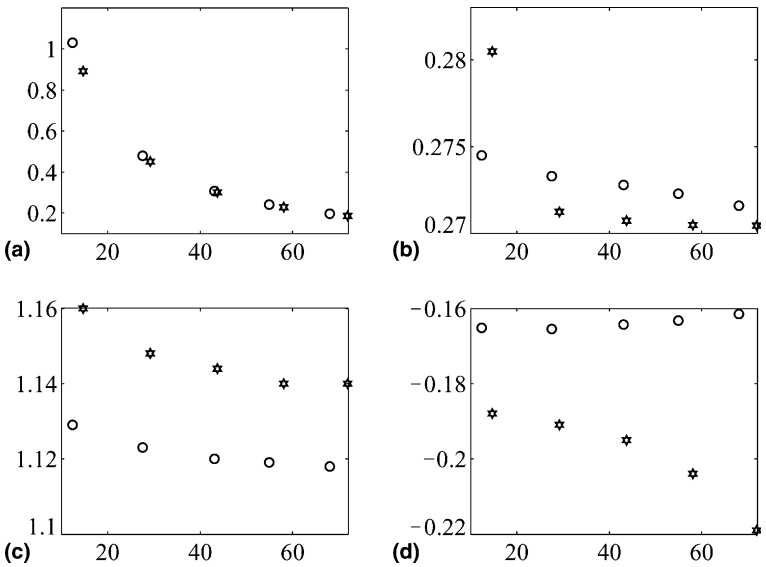

Fig. 6. Comparison between the computed results (stars) and the ones in [7,9] (circles) for different Reynolds numbers; (a) dimensionless pressure drop $\Delta P/\rho\langle u\rangle^2$; (b) lateral position y_c of the disc; (c) disc velocity to mean velocity ratio $U/\langle u\rangle$; (d) dimensionless angular velocity of the disc $\omega R/\langle u\rangle$.

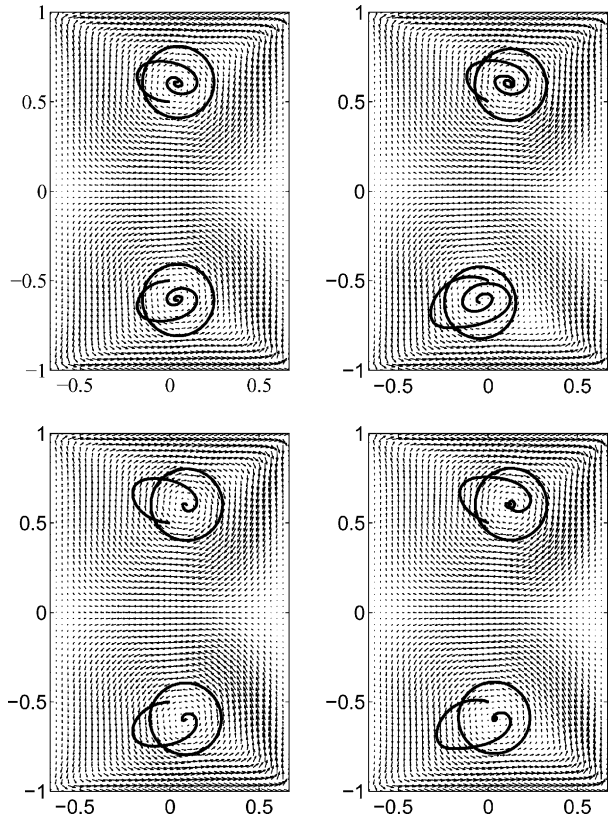

Fig. 7. Motion of two discs in a lid-driven $4/3 \times 2$ cavity. The lower and upper walls of the cavity are moved with the velocities $U_{\text{lid}} = 50$ (upper row) and $U_{\text{lid}} = 100$ (lower row); $\rho_{\text{f}} = 1$, $\rho_{\text{s}} = 0.5$, $\mu = 1$, $g = 0$ (left), $g = 700$ (right), $R = 0.2$. The spirals are trajectories of the centers of the discs.

the equilibrium point of the upper disc moves to the right and the equilibrium point of the lower disc moves to the left. In spite of the fact that the pressure does not appear explicitly in Eq. (5) the body–pressure interaction is due to the pressure correction that is applied to the fluid that is formally inside the discs.

The present study was inspired by the investigation of advection of neutrally buoyant discs in a two-dimensional chaotic lid-driven cavity flow at zero Reynolds number [10]. The schematic view of a 3×2 cavity is presented in Fig. 8. In order to simulate a Stokes flow, the above algorithm was slightly modified. The advection step is irrelevant in this case, and Eqs. (3) and (5) for pressure and velocity were iterated until their stabilization at each time step. In order to control the precision of the calculations, we used grids with different spatial resolutions from 75×50 to 240×160. Regarding the solution on the finest grid as an "exact" we have computed L_2-norm error for the solutions obtained on the coarser grids. Since in the Stokes flow the flowfield depends only on the current configuration and does not depend on the history of the system, the error was calculated for some initial moment of time. The results are presented in Fig. 9, and it can be seen that the proposed method has second-order accuracy with respect to the step of the grid.

We considered motion of free equal discs with dimensionless radii 0.15. In the absence of the discs there are two counter-rotating vortices, one due to the motion of the upper wall, and the second due to the motion of the lower wall. If the velocities of the walls are constant a disc should be trapped by lower or upper vortex. Since the discs have a finite size, they affect the flow and make it time-dependent. Time-

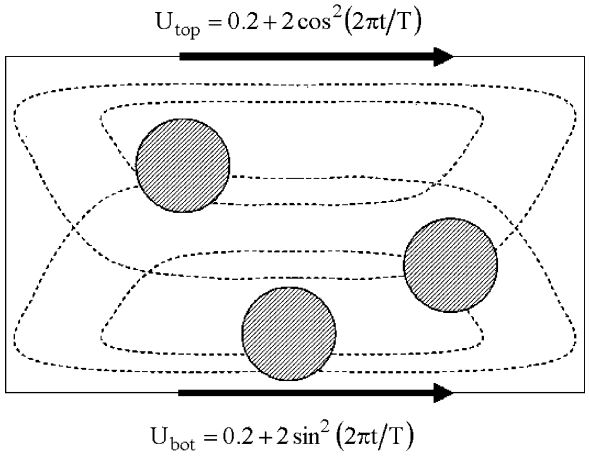

Fig. 8. Schematic view of a cavity flow driven by moving walls.

periodic forcing makes it possible for the particles to pass from one vortex to the other. We have examined a particular form of the forcing that is shown in Fig. 8. The positions of the discs centers after each period form Poincaré sections that are presented in Fig. 10. Note, that unlike passive tracers, finite-size bodies do not follow the liquid. The latter is the reason that the points at the Poincaré sections condense into clusters. For small values of period T, a disc is trapped by a vortex and does not have time to cross the boundary between two vortices (Fig. 10(a)). Although the trajectories of the discs are chaotic, they do not intertangle. When $T \approx 1.6\pi$ the dynamics of the system changes drastically, the particles pass from one vortex to the

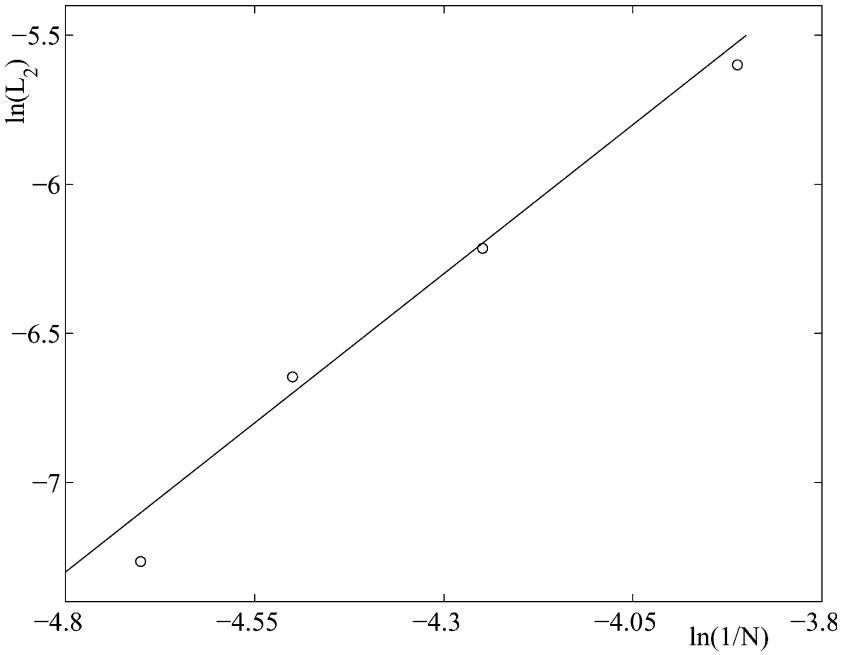

Fig. 9. L_2-norm of an error at the initial moment of time vs. number of nodes: ○, the solid line has slope equal to 2.

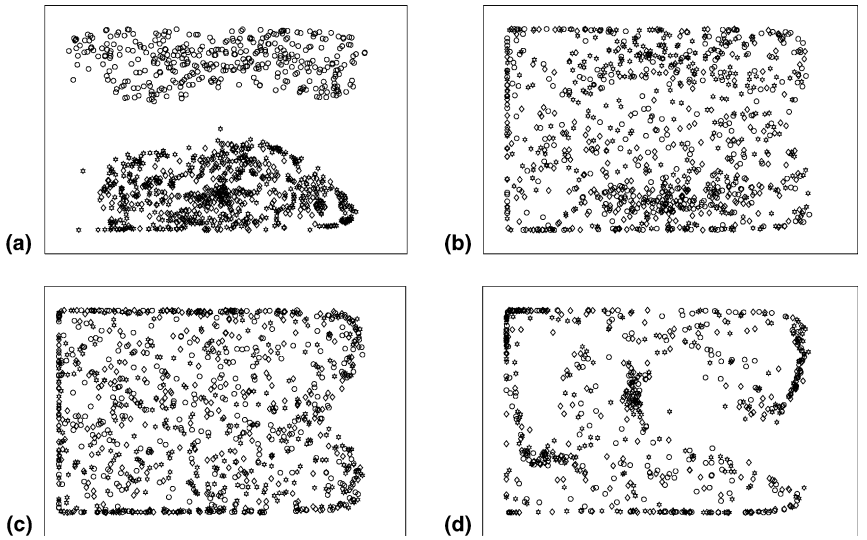

Fig. 10. Poincaré section: (a) $T = \pi$, (b) $T = 1.6\pi$, (c) $T = 1.7\pi$, (d) $T = 2\pi$. Each disc is denoted by different symbol, namely circle, rhombus, and star.

other, and rotate counter and clockwise. Due to the rotation in opposite directions the trajectories of the discs tangle and form braids in the augmented (x, y, t) phase space.

4. Conclusion

In the present study, we have proposed a variant of the immersed boundaries method that allows the direct numerical simulation of fluid–solid flows on a regular rectangular grid. The method models a no-slip boundary with the second-order accuracy interpolation scheme without explicit calculation of the forces that the particles exert at the fluid. Unlike the DLM method that treats the particles–fluid interaction via constrained variational equations, the interpolation scheme leads to unconstrained minimization problems. From the physical point of view the Lagrange multipliers enforce the non-slip boundary conditions only at the end of the iteration procedure. Thus, the flowfield at an intermediate iteration does not satisfy the boundary condition, while the proposed interpolation method matches the fluid velocity with the body velocity at any iteration. In order to test its performance the method was applied to simulation of the motion of a periodic chain of neutrally buoyant particles in pressure-driven Poiseuille flow. The obtained results are in good agreement with the results reported in the literature. The method is applicable for wide range of Reynolds numbers from creeping flows up to $Re \approx 100$, applicability of this method to direct simulation of two phase turbulent flows should be subject of additional investigations. While the method was applied to two-dimensional flow of discs, it can be easily extended to bodies of arbitrary configuration as well as to a three-dimensional geometry.

Acknowledgements

We thank the anonymous Referees for numerous helpful suggestions.

References

[1] H.H. Hu, N.A. Patankar, M.Y. Zhu, Direct numerical simulations of fluid–solid systems using the arbitrary Lagrangian–Eulerian technique, J. Comput. Phys. 169 (2001) 427.
[2] A.J.C. Ladd, R. Verberg, Lattice-Boltzmann simulations of particle fluid suspensions, J. Stat. Phys. 104 (2001) 1191.
[3] E.A. Fadlun, R. Verzicco, P. Orlandi, J. Mohd-Yusof, Combined immersed-boundary finite-difference methods for three-dimensional complex flow simulations, J. Comput. Phys. 161 (2000) 35.
[4] C.S. Peskin, Flow patterns around heat valves: a numerical method, J. Comput. Phys. 10 (1972) 252.
[5] E.M. Saiki, S. Biringen, Numerical simulation of a cylinder in uniform flow: application of a virtual boundary method, J. Comput. Phys. 123 (1996) 450.
[6] R. Glowinski, T.-W. Pan, T. Hesla, D.D. Joseph, J. Periaux, A fictious domain approach to the direct numerical simulation of incompressible viscous flows past moving rigid bodies: application to particulate flow, J. Comput. Phys. 169 (2001) 363.
[7] T.-W. Pan, R. Glowinski, Direct simulation of the motion of neutrally buoyant circular cylinders in plane Poiseulle flow, J. Comput. Phys. 181 (2002) 260.
[8] F. Gibou, R.P. Fedkiw, L.-T. Cheng, M. Kang, A second-order symmetric discretization of the poisson equation on irregular domain, J. Comput. Phys. 176 (2002) 205.
[9] T. Inamuro, K. Maeba, F. Ogino, Flow between parallel walls containing the lines of neutrally buoyant circular cylinders, Int. J. Multiphase Flow 26 (2000) 1981.
[10] A. Vikhansky, Chaotic advection of finite-size bodies in a cavity flow, Phys. Fluids 15 (2003) 1830.